International Journal of the Korean Society of Precision Engineering, Vol. 3, No. 2, April 2002.

Dynamic Characteristics of Indeterminate Rotor Systems with Angular Contact Ball Bearings Subject to Axial and Radial Loads

Seong-Wook Hong[1], Joong-Ok Kang[2] and Yung C. Shin[3]

[1] School of Mechanical Engineering, Kumoh National University of Technology, Kumi, Korea
[2] Graduate School, Kumoh National University of Technology, Kumi, Korea
[3] School of Mechanical Engineering, Purdue University, West Lafayette, U.S.A.

ABSTRACT

This paper presents the dynamic analysis of indeterminate rotor systems with angular contact ball bearings subject to axial and radial loads. The reaction forces against applied radial loads significantly influence the dynamic characteristics of angular contact ball bearings. However, the reaction forces are hard to determine in the case of indeterminate rotor-bearing systems. To this end, this paper proposes a finite element model for indeterminate rotor systems with angular contact ball bearings. An improved bearing model is adopted which is originated from the Harris's bearing dynamic model. The bearing model is also extended to include centrifugal forces due to the ball and inner ring. This paper utilizes a new iterative algorithm for general, indeterminate rotor systems with angular contact ball bearings. Two examples are provided to illustrate the dynamic characteristics of rotor systems with angular contact ball bearings subject to axial and radial loads. The experimental and numerical results prove that the proposed method is useful for the dynamic analysis of indeterminate rotor systems with angular contact ball bearings.

Keywords : Rotor-bearing system, Angular contact ball bearing (ACBB), Indeterminate system, Reaction forces, Finite element method (FEM), Radial load, Axial load

1. Introduction

Angular contact ball bearing (ACBB) is often adopted for rotating machinery such as machine tool spindle because of the inherent capability to sustain both the axial and radial loads. In particular, increasing demand toward the high productivity and accuracy has attracted a great attention into spindle dynamics involved with angular contact ball bearings (ACBBs) [1-9]. However, difficulty still remains to assess accurate dynamic parameters of ACBBs subject to axial and radial loads. Since the dynamic parameters of ACBBs are changed by where and how ACBBs are placed [9,10], the bearing parameters often become the major source to degrade the accuracy in the dynamic analysis of rotor systems with ACBBs. It is well known from the literature that the reaction forces of bearings to applied radial loads significantly influence the dynamic characteristics of ACBB. However, the reaction forces are often hard to determine in the case of indeterminate rotor systems. Then, determination of bearing stiffness coefficients requires a systematic approach to reflect the fact that bearing characteristics affect the reaction forces and in turn the reaction forces affect the bearing characteristics. Several papers, mostly based on simple, ideal rotors, have attempted integrated modeling methods and have shown the bearing and shaft interaction has a

significant role in the dynamics of rotor systems with ACBBs [7-9]. However, few research works have been general enough to take account of complicated configurations of actual rotor-bearing systems.

The dynamic model of ACBB has evolved for several decades so as to account for crucial terms. State-

of-the-art bearing dynamic models are described in the literature, e.g., [1,11,12]. Although the dynamic characteristics of ACBB are affected by many parameters such as axial preload, rotational speed, external radial load, temperature, etc., the primary concern of this paper is the effect of axial and radial loads on bearing characteristics, which often becomes a critical issue for indeterminate rotor-bearing systems. In this paper, a finite element model is developed which can be used for general, indeterminate rotor systems with ACBBs subject to axial and radial loads. An iterative algorithm is proposed to solve the integrated equations of indeterminate rotor-bearing systems. This paper adopts the bearing dynamic model developed in [1], but replaces the influence coefficient method in [1] by the finite element method for shaft modeling. In addition, this paper resolves two major limitations in existing methods: i.e., the inability to rotor systems with more than two bearings and the disregard of the coupling effects between horizontal and vertical directions.

Two examples are provided to investigate the dynamics of indeterminate rotor systems with ACBBs as well as to validate the proposed method. The experimental and numerical studies show that the proposed method is useful for the dynamic analysis of general rotor systems with ACBBs.

2. Modeling of Rotor System with Angular Contact Ball Bearings

2.1 The Finite Shaft Element and Rigid Disk Element

The finite element method has become an essential tool for the dynamic analysis of rotor-bearing systems [13,14] and has been applied also to rotor systems with ACBBs by several researchers [2-6]. The standard finite element model of a rotor-bearing system consists of three fundamental elements, i.e. finite length shaft, rigid disk and discrete bearing.

Neglecting the internal and external damping of the shaft, the matrix equation of motion for a finite shaft element can be expressed as

$$\begin{bmatrix} m^s & 0 \\ 0 & m^s \end{bmatrix}\begin{Bmatrix} \ddot{y}^s \\ \ddot{z}^s \end{Bmatrix}+\Omega\begin{bmatrix} 0 & g^s \\ -g^s & 0 \end{bmatrix}\begin{Bmatrix} \dot{y}^s \\ \dot{z}^s \end{Bmatrix}+\begin{bmatrix} k^s & 0 \\ 0 & k^s \end{bmatrix}\begin{Bmatrix} y^s \\ z^s \end{Bmatrix}=\begin{Bmatrix} f_y^s \\ f_z^s \end{Bmatrix} \tag{1}$$

where Ω denotes the rotational speed, and the superscript s denotes the shaft element. $\{y^s\}$ and $\{z^s\}$ represent the 4x1 nodal coordinate vectors in the XY and XZ planes, respectively, and the force vectors, $\{f_y^s\}$ and $\{f_z^s\}$, include all kinds of forces influencing the shaft element.

The rigid, discrete disk, assuming that it is thin and symmetric about the axis of rotation, has the equation of motion

$$\begin{bmatrix} m^d & 0 \\ 0 & m^d \end{bmatrix}\begin{Bmatrix} \ddot{y}^d \\ \ddot{z}^d \end{Bmatrix}+\Omega\begin{bmatrix} 0 & g^d \\ -g^d & 0 \end{bmatrix}\begin{Bmatrix} \dot{y}^d \\ \dot{z}^d \end{Bmatrix}=\begin{Bmatrix} f_y^d \\ f_z^d \end{Bmatrix} \tag{2}$$

Nomenclature

d_m = bearing pitch diameter
E = elastic modulus
f = force vector
F = load vector
F_c = centrifugal force
g = gyroscopic matrix
J = Jacobian matrix
k = stiffness matrix
K = load-deflection parameter
l = ball and groove center separation
m = mass matrix
M = moments
Q = load vector, contact load
r = radial direction
R = right eigenvector
$R\phi$ = transformation matrix
y,z = nodal coordinate vectors
u = displacement vector, inner ring groove center displacement
u_{cent} = inner ring motion due to centrifugal force
v = ball center displacement
x = axial direction
α = contact angle
β = ball rotational angle
γ = angular displacement
δ = displacement vector
λ = eigenvalue
ν = Poisson's ratio
θ = angular displacement
ρ = density
ρ_i = inner groove center radius
σ = diameter ratio
ω_c = ball orbital speed
Ω = rotational speed

Superscripts
b = bearing element
d = disk element
s = shaft element
T = transpose

Subscripts
e = outer ring
i = inner ring
j = refers to j-th ball
o = initial

where the superscript d denotes the disk, $\{y^d\}$ and $\{z^d\}$ represent the 2x1 nodal coordinate vectors in the XY and XZ planes, respectively, and $\{f_y^d\}$ and $\{f_z^d\}$ are the corresponding force vectors. The element matrices for equations (1) and (2) are well described in the literature, e.g., [13,14].

2.2 Bearing Dynamic Model

This paper adopts the bearing model introduced in [1,9]. However, thermal expansion is not taken into account in this paper. The following assumptions are placed on the bearing model.

① Friction, cage forces, and thermal expansion are ignored.
② Gyroscopic moments do not affect contact deformation.

Fig. 1 shows a schematic model for ACBB [9]. The displacement vectors for the bearing center and inner ring groove center are defined, respectively, as

$$\{\delta\} = \{\delta_x \quad \delta_y \quad \delta_z \quad \gamma_y \quad \gamma_z\}^T \tag{3-1}$$

$$\{u\} = \{u_r \quad u_x \quad \theta\}^T = [R\phi]\{\delta\} \tag{3-2}$$

and the corresponding load vectors are

$$\{F\} = \{F_x \quad F_y \quad F_z \quad M_y \quad M_z\}^T = [R\phi]^T\{Q\} \tag{4-1}$$

$$\{Q\} = \{Q_r \quad Q_x \quad M\}^T \tag{4-2}$$

The transformation matrix for the local frame to the global frame is defined as

$$[R\phi] = \begin{bmatrix} 0 & \cos\phi & \sin\phi & -x_p\sin\phi & x_p\cos\phi \\ 1 & 0 & 0 & r_p\sin\phi & -r_p\cos\phi \\ 0 & 0 & 0 & -\sin\phi & \cos\phi \end{bmatrix} \tag{5}$$

where ϕ is the angle between the vertical line and the ball center line from the bearing center. Motions of the ball center and ring groove centers are shown in Fig. 2 [9]. Then, the contact angles α are determined by

$$\tan\alpha_e = \frac{l_{oe}\sin\alpha_o + v_x}{l_{oe}\cos\alpha_o + v_r}$$

$$\tan\alpha_i = \frac{l_{oi}\sin\alpha_o + u_x - v_x}{l_{oi}\cos\alpha_o + u_r - v_r + u_{cent}} \tag{6}$$

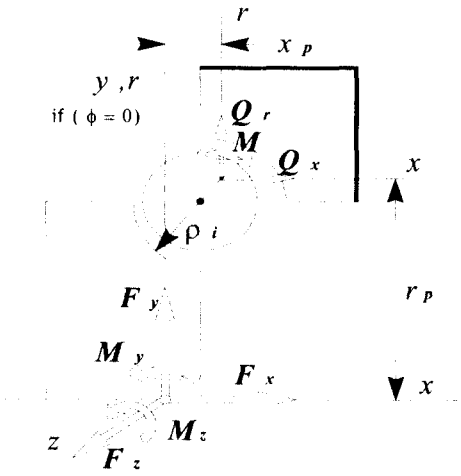

(a) Geometry and loading

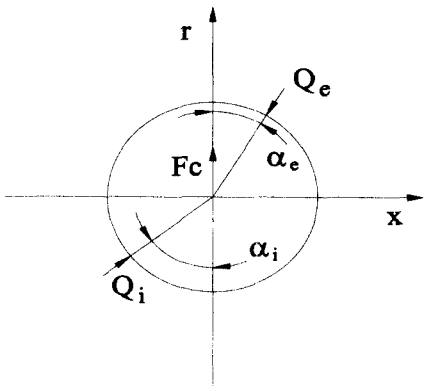

(b) Contact angles for a ball

Fig. 1 Schematic model of angular contact ball bearing

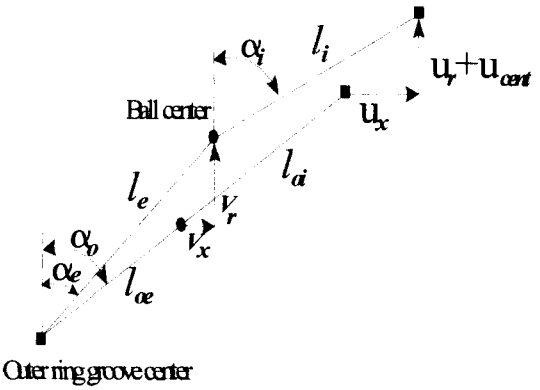

Fig. 2 Schematic diagram for representing the ball center and inner ring groove center movements

where

$$l_i = \left[(l_{oi}\cos\alpha_o + u_r - v_r + u_{cent})^2 + (l_{oi}\cos\alpha_o + u_x - v_x)^2\right]^{1/2}$$
$$l_e = \left[(l_{oe}\cos\alpha_o + v_r)^2 + (l_{oe}\sin\alpha_o + v_x)^2\right]^{1/2}$$

Here α_0 , l , l_0 are the initial contact angle, the deformed center length and the initial center length, respectively, and v , u are the ball center motion and the inner ring motion, respectively, u_{cent} being the inner ring motion due to centrifugal force. Ball-raceway deformation is the change of center length, assuming no clearances exist:

$$\delta_i = l_i - l_{oi} \ , \ \delta_e = l_e - l_{oe} \tag{7}$$

Contact loads are calculated with Hertzian theory for spherical contact:

$$Q_i = K_i\delta_i^{3/2} \ , \ Q_e = K_e\delta_e^{3/2} \tag{8}$$

where K_i , K_e are the load-deflection parameters [11]. On the other hand, ball centrifugal force can be written as

$$F_c = \frac{1}{2}md_m\omega_c^2 \tag{9}$$

where ω_c is the ball orbital speed that can be approximated as

$$\omega_c = \Omega\left[1+\frac{(\sigma+\cos\alpha_e)\cos(\alpha_i-\beta)}{(\sigma-\cos\alpha_i)\cos(\alpha_e-\beta)}\right]^{-1} \tag{10}$$

The ball spinning axis angle with respect to the bearing center axis can be determined by

$$\tan\beta = \frac{\sigma\sin\alpha_e}{1+\sigma\cos\alpha_e} \tag{11}$$

where σ is the ball diameter divided by the bearing pitch diameter.

Then, the load equilibrium at the ball is given by

$$\begin{aligned}\sum F_r &= Q_i\cos\alpha_i - Q_e\cos\alpha_e + F_c = 0\\ \sum F_x &= Q_i\sin\alpha_i - Q_e\sin\alpha_e = 0\end{aligned} \tag{12}$$

Equation (12) is nonlinear equations to be solved for each ball. The ball Jacobian matrix $[J_b] = \partial\{F\}/\partial\{v\}$ is found by differentiating equation (12):

$$[J_b] = [J_e] + [J_i] \tag{13}$$

where

$$[J_e] = \begin{bmatrix} -\frac{\partial Q_e}{\partial\delta_e}\cos^2\alpha_e - \frac{Q_e}{l_e}\sin^2\alpha_e & \left(\frac{Q_e}{l_e} - \frac{\partial Q_e}{\partial\delta_e}\right)\sin\alpha_e\cos\alpha_e \\ \left(\frac{Q_e}{l_e} - \frac{\partial Q_e}{\partial\delta_e}\right)\sin\alpha_e\cos\alpha_e & -\frac{\partial Q_e}{\partial\delta_e}\sin^2\alpha_e - \frac{Q_e}{l_e}\cos^2\alpha_e \end{bmatrix}$$

$$[J_i] = \begin{bmatrix} -\frac{\partial Q_i}{\partial\delta_i}\cos^2\alpha_i - \frac{Q_i}{l_i}\sin^2\alpha_i & \left(\frac{Q_i}{l_i} - \frac{\partial Q_i}{\partial\delta_i}\right)\sin\alpha_i\cos\alpha_i \\ \left(\frac{Q_i}{l_i} - \frac{\partial Q_i}{\partial\delta_i}\right)\sin\alpha_i\cos\alpha_i & -\frac{\partial Q_i}{\partial\delta_i}\sin^2\alpha_i - \frac{Q_i}{l_i}\cos^2\alpha_i \end{bmatrix}$$

The inner ring expansion due to the centrifugal force can be approximated as

$$u_{cent} = \frac{\rho\Omega^2}{32E}d_m\left[D_i^2(3+\nu) + d_m^2(1-\nu)\right] \tag{14}$$

where E, ν are the elastic modulus and the Poisson's ratio, respectively. It is assumed here that the inner ring expansion can be simply superimposed into the inner ring center displacement as shown in Fig. 2.

Global force equilibrium is established in terms of bearing loading and ball reaction forces at the bearing centroid.

$$\{F\} + \sum_{j=1}^{n}[R\phi]_j^T\{Q\}_j = \{0\} \tag{15}$$

where n is the number of balls. The bearing boundary conditions have an important effect on the numerical solution of equation (15). When loading is given, there are five unknown displacements. Conversely, if displacements are known, loads may be found directly without iteration once equation (12) is solved for each ball. However, in this paper, mixed boundary condition is taken into account to be able to apply two kinds of axial preloads: constant force preload method and constant displacement method. A nonlinear solver based on the Powell hybrid method [15] is used for solving equations (12) and (15). The nonlinear solver is recursively applied for equation (12) and then equation (15) until both equations are satisfied within the specified tolerance.

Bearing stiffness matrix can be found from the Jacobian matrix, using the ball Jacobian matrices:

$$\underset{5\times5}{K^b} = \left[\frac{\partial\{F\}}{\partial\{\delta\}}\right] = -\sum_{j=1}^{n} \underset{5\times3}{[R\phi]_j^T} \; diag \{ \underset{3\times3}{[J_e]} \underset{3\times3}{[J_b]^{-1}} \underset{3\times5}{[J_i],0} \} \underset{3\times5}{[R\phi]_j} \quad (16)$$

Bearing stiffness matrix formula (16) requires the ball Jacobian matrices that should be determined with the solutions of equations (12) and (15).

Thus, an ACBB can be modeled, assuming axial motion is negligible, as 16 spring coefficients (10 different coefficients): i.e.,

$$\begin{bmatrix} k_{yy}^b & k_{y\theta_z}^b & k_{yz}^b & k_{y\theta_y}^b \\ k_{y\theta_z}^b & k_{\theta_z\theta_y}^b & k_{\theta_z z}^b & k_{\theta_z\theta_y}^b \\ k_{yz}^b & k_{\theta_z z}^b & k_{zz}^b & k_{z\theta_y}^b \\ k_{y\theta_y}^b & k_{\theta_z\theta_y}^b & k_{z\theta_y}^b & k_{\theta_y\theta_y}^b \end{bmatrix} \begin{Bmatrix} y^b \\ z^b \end{Bmatrix} = \begin{Bmatrix} f_y^b \\ f_z^b \end{Bmatrix} \quad (17)$$

where the superscript b denotes the bearing, K_{ij}^b are the linearized i directional stiffness due to j directional motion. $\{y^b\}$, $\{z^b\}$ are the 2x1 nodal coordinate vectors in the XY and XZ planes, respectively, $\{f_y^b\}$ and $\{f_z^b\}$ being the corresponding 2x1 force vectors. The off-diagonal components are generally small unless a significant amount of load is applied.

2.3 The Global System Equation and the Associated Problems

For a typical rotor system with ACBBs, assembling of the element matrices as described in equations (1), (2) and (17) provides a finite element equation of motion:

$$[M_o]\{\ddot{q}\} + \Omega[G_o]\{\dot{q}\} + \{[K_o] + [K_b]\}\{q\} = \{f\} \quad (18)$$

where $\{q\}$ and $\{f\}$ are the global coordinate vector and the force vector, respectively. The subscripts b and o represent the system matrices composed of bearing elements and the others, respectively.

To determine the reaction forces of bearings to applied static radial loads, the corresponding static equation should be solved. Elimination of the mass and damping terms out of equation (18) yields

$$\{[K_o] + [K_b]\}\{q\} = \{f\} \quad (19)$$

By solving equation (19), one may have information on shaft deflection and reaction forces at bearings against static radial loads. Equation (19) is used for updating bearing reaction forces and moments in the solution procedure that will be described in the next section. Equation (18) can be rewritten, in state form, as

$$[A]\{\dot{Q}\} + [B]\{Q\} = \{F\} \quad (20)$$

where

$$[A] = \begin{bmatrix} 0 & M_o \\ M_o & C_b + \Omega G_o \end{bmatrix}, \; [B] = \begin{bmatrix} -M_o & 0 \\ 0 & K_o + K_b \end{bmatrix}$$

The eigenvalue problem associated with equation (20) can be written as

$$\{\lambda_i [A] + [B]\}\{R_i\} = \{0\} \quad (21)$$

where λ_i, $\{R_i\}$ are the i-th eigenvalue and the corresponding right eigenvector, respectively.

2.4 The Solution Procedure

Since the bearing coefficients are affected by external radial loads applied to the bearings, the reaction forces of bearings are required to be determined in advance for obtaining the bearing coefficients. If the system is determinate, in other words, the number of bearings is two and moment stiffness coefficients of bearings are negligible, the solution procedure is straightforward. Then, the reaction forces against radial loads can be determined only from the static force equilibrium relation. On the other hand, if a rotor system has more than two bearings and/or moment stiffness coefficients of bearings are not negligible, the bearing reaction forces are related implicitly with bearing stiffness coefficients because of the inherent indeterminate nature. One of the possible solution methods to this indeterminate problem is to solve all the equations at the same time as taken in [6]. This is a straightforward method but requires a lot of computational effort to solve many complicated nonlinear equations simultaneously. Jorgensen [1] proposed an attractive iterative algorithm, which

determines an initial reaction force distribution of bearings assuming no moment (tilt) stiffness coefficients are present. Although the algorithm has been proved successful, it is limited to the case when the number of bearings is only two. To remove this limitation, this paper proposes a new iterative algorithm as summarized below:

① Assess the initial bearing stiffness coefficients by solving bearing equations (10) and (15) with disregarding the interaction between the shaft and bearings due to radial loads.
② Solve and obtain the reaction forces and moments of bearings from the static force deformation equation (19) of the system with the bearing stiffness coefficients determined in the previous step.
③ Put the reaction forces and moments into the bearing equations to determine new bearing stiffness coefficients.
④ Substitute the old coefficients by the new ones and go to step (2).
⑤ Iterate the above three steps until the bearing stiffness coefficients are converged. The number of iterations is significantly dependent upon the complexity of the system and the number of finite elements.
⑥ Solve the eigenvalue problem as given in equation (21)

3. Validation and Illustration of the Proposed Method

3.1 A Uniform Shaft Supported by Two ACBBs

A simple experimental system is established to validate the proposed method. Fig. 3 shows the experimental setup. A uniform shaft, of which length and diameter are 80 cm and 2.5 cm, respectively, is supported by two identical ACBBs. Table 1 shows the specifications of the bearings used in the experiment.

The system is equipped with a device to apply axial force preload to the system. The photo in Fig.3 shows the preload device. The preload device is made of a spring and a bolt to compress the spring. The bolt is used to adjust axial force preload. Fig. 4 compares the first three natural frequencies from the experiment and simulation with the axial force load varied.

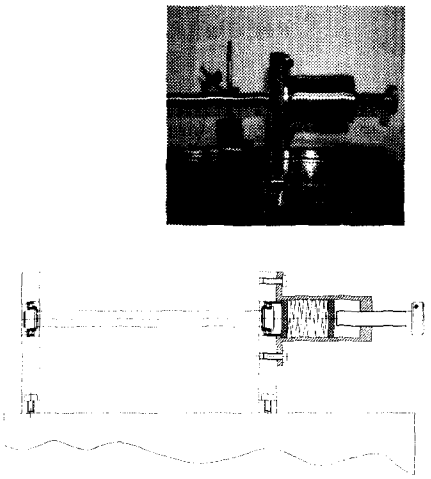

Fig. 3 Experimental setup for a uniform shaft supported by two bearings

Table 1 Bearing data for the uniform shaft system

Property	Data
Type	7006C
Pitch diameter (mm)	42.5
Number of balls	14
Width (mm)	13
Ball diameter (mm)	6
Initial contact angle (deg)	15
Groove curvature radius/Ball diameter	0.5199

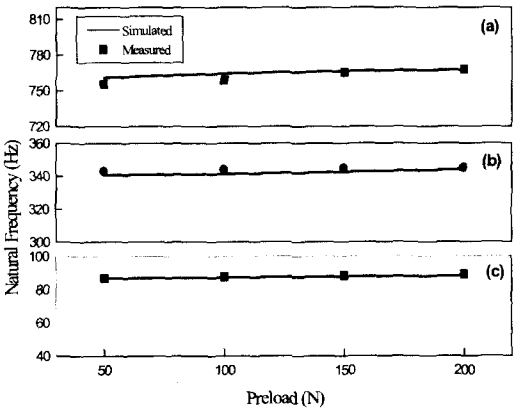

Fig. 4 Comparison of the first three natural frequencies from simulation and experiment for the uniform shaft system: (a) First; (b) Second; (c) Third

The figure shows that the simulation results are in good agreement with the experimental results. Both the simulation and experiment show that axial preload increases natural frequencies. Measured and computed modes shapes are compared in Fig. 5, which also proves the adequacy of the model

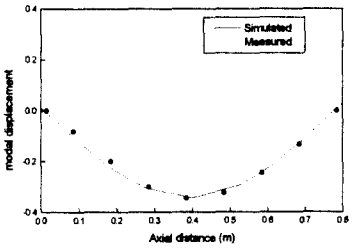

(a) first

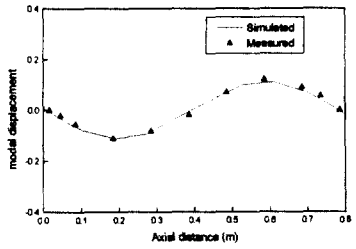

(b) second

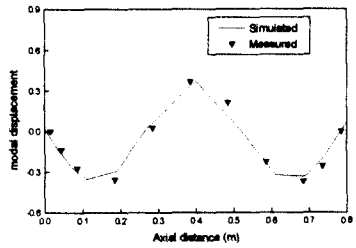

(c) third

Fig. 5 Comparison of measured and computed mode shapes for the uniform shaft system

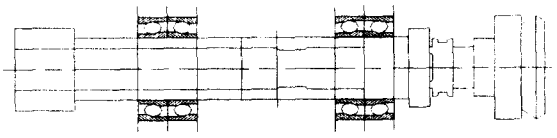

Fig. 6 A spindle bearing model

Table 2 Specifications of the spindle-bearing system (model 1)

Element	Data			
Shaft	Density, kg/m^3		7800	
	Elastic modulus, N/m^2		2.10E11	
	Element #	Outer Dia.(m)	Inner Dia.(m)	Element Length (m)
	1	0.09	0.045	0.057
	2	0.07	0.045	0.047
	3	0.0823	0.045	0.02
	4	0.0823	0.045	0.02
	5	0.07	0.045	0.0492
	6	0.07	0.045	0.0492
	7	0.07	0.040	0.0304
	8	0.07	0.045	0.0398
	9	0.0823	0.045	0.012
	10	0.0823	0.0135	0.014
	11	0.0823	0.0135	0.014
	12	0.07	0.0135	0.014
	13	0.0848	0.0135	0.0204
	14	0.0443	0.0	0.0026
	15	0.061	0.0	0.016
	16	0.0445	0.0	0.0175
	17	0.0555	0.0	0.0155
	18	0.0815	0.0	0.018
	19	0.06	0.0	0.007
	20	0.081	0.066	0.018
Bearings (4 identical)	Positions Double bearings at each		Node 5 (rear) Node 12(front)	
	Type		7014	
	Pitch diameter (mm)		90	
	Number of balls		20	
	Ball diameter (mm)		11.9	
	Initial contact angle(deg)		15	
	Groove curvature radius/Ball diameter		0.5199	

Table 3 Comparison of bearing stiffness coefficients computed from the current and Jorgensen's methods: subjected to axial displacement preload of 14.9 μ m and radial load of 100 N in the y direction.

Brg	Method	k_{yy} GN/m	k_{zz} GN/m	$k_{\theta_y\theta_y}$ KNm/rad	$k_{\theta_z\theta_z}$ KNm/rad
Rear	Jorgensen	3179.1	3179.2	61.827	61.826
	Current	3179.0	3179.2	61.827	61.825
Front	Jorgensen	3178.4	3178.9	61.822	61.810
	Current	3178.1	3178.9	61.820	61.805

Table 4 Comparison of natural frequencies computed from the current and Jorgensen's methods: subjected to axial displacement preload of 14.9 μ m and radial load of 100 N in the y direction.

Speed rpm	Method	Mode 1 Hz	Mode 2 Hz	Mode 3 Hz
0	Jorgensen	1010.2	1180.9	1962.8
	Current	1019.0 1019.1	1153.0 1153.1	2011.0 2011.1
2000	Jorgensen	1011.9	1182.2	1966.4
	Current	1018.8 1021.2	1152.0 1155.1	2011.3 2014.7

3.2 A Spindle-Bearing System

In order to validate the proposed method and to investigate the dynamics of a realistic rotor system with ACBBs, a spindle-bearing model for Mazak CNC vertical milling machine with a small tool [1,9] is considered as the next example. The system is shown in Fig. 6. This spindle has four ACBBs: two pairs of ACBBs. Each pair constitutes so called 'o' configuration.

Two numerical models are made for the current system. In order to compare the proposed method with the Jorgensen's method [1], numerical model 1 is established in the same manner as that in [1]: i.e., two neighboring bearings are placed at the same node. The detailed specifications of model 1 are given in Table 2. On the other hand, the other numerical model (model 2) is constructed by making a minor modification to model 1. The only difference between model 1 and model 2 is that each bearing is placed at a different node.

At first, a simulation is performed with model 1 under an external radial load of 100 N at the last node of spindle and a constant axial displacement preload of 14.9 μ m at all the bearings. Table 3 compares bearing stiffness coefficients computed from the proposed method and the Jorgensen's method. The stiffness coefficients from the proposed method are almost identical to those from the Jorgensen's method. Table 4 compares natural frequencies computed from two methods. There is 1~2 % difference, which is believed to occur due to the difference in modeling techniques for shaft elements: the finite element method in the proposed method and the influence coefficient method in the Jorgensen's work. This result assures that the proposed method can provide as good results as the Jorgensen's method. In addition, the number of natural frequencies from the present method is twice that of the Jorgensen's method. The reason is that the proposed method considers both the vertical and horizontal motions while the Jorgensen's model takes consideration of only one plane motion.

To see the effects of ball centrifugal force and inner ring expansion due to centrifugal force on bearing stiffness, Fig. 7 illustrates the variation of direct stiffness k_{yy} of the rear bearing with and without those effects. Constant axial displacement preload of 14.9 μ m is applied at all the bearings. It is clearly shown that the ball centrifugal force is softening the bearing while the inner ring expansion is stiffening the bearing. Fig. 8 illustrates the variation of k_{yy} of the rear bearing with the axial preload varied. The direct stiffness coefficient tends to increase as the axial preload increases but decrease as the rotational speed increases.

On the other hand, radial load effect is investigated by applying a radial load at the front end of the spindle. Fig. 9 shows the direct stiffness coefficients of bearings when a radial load of 500 N is applied to the front end of the spindle. The bearing stiffness coefficients obviously exhibit anisotropy, which, however, has been usually disregarded in the dynamic analysis of spindle-bearing systems.

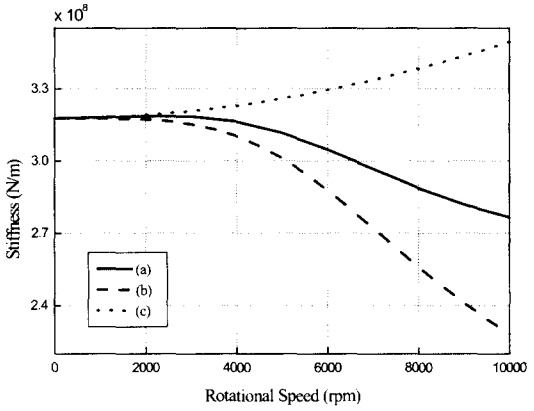

Fig. 7 Comparison of k_{yy} : (a) with both ball and inner ring centrifugal forces; (b) with only ball centrifugal force; (c) with only inner ring centrifugal force.

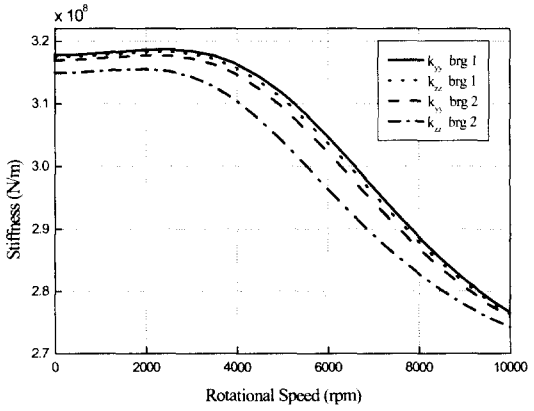

Fig. 8 Direct stiffness coefficient k_{yy} with axial preload varied.

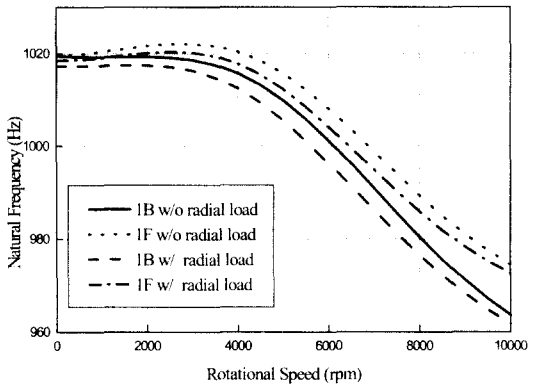

Fig. 9 Comparison of k_{yy}, k_{zz} when a radial load of 500 N is applied at the front end of the spindle.

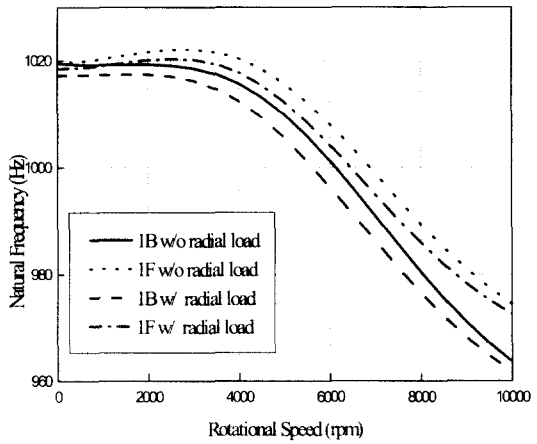

Fig.10 The first two natural frequencies with/without radial load of 500N at the front end of the spindle.

In this case, natural frequencies are split with respect to the rotational speed, due not only to gyroscopic effect but also to bearing anisotropy. Fig. 10 shows the first forward and backward natural frequencies with and without the radial load of 500 N. Two distinct natural frequencies are observed even at the stationary condition because of the bearing anisotropy arising due to the radial load.

Next, a simulation is performed with model 2. As mentioned in the previous section, rotor systems with more than 2 ACBBs are not solvable with the Jorgensen's method. Thus, in this case, only the current program is run with an axial displacement preload of 14.9 μ m and a radial load of 500 N at the front end of the spindle. The results are presented in Table 5.

Table 5 Comparison of bearing stiffness coefficients from model 1 and model 2: subjected to axial displacement preload of 14.9 μ m and radial load of 500 N in the y direction.

Model 1 #	Bearing	k_{yy} GN/m	k_{zz} GN/m	$k_{\theta_y\theta_y}$ KNm/rad	$k_{\theta_z\theta_z}$ KNm/rad
1*	Rear 1 Rear 2	0.3174 40.317 44	0.3177 60.317 76	61.804 61.804	61.755 61.755
2**	Rear 1 Rear 2	0.3175 20.317 43	0.3177 90.317 76	61.808 61.803	61.767 61.752
1	Front 1 Front 2	0.3149 10.314 91	0.3169 30.316 93	61.716 61.716	61.486 61.486
2	Front 1 Front 2	0.3153 40.314 63	0.3170 70.316 84	61.733 61.703	61.539 61.448

* Two neighboring bearings are placed at the same node.

** Each bearing is placed at a different node.

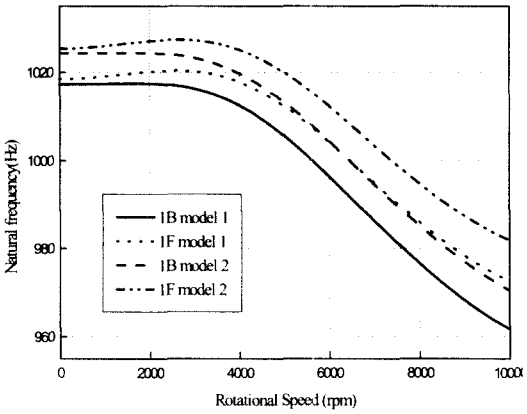

Fig. 11 Comparison of the first two natural frequencies computed from model 1 and model 2 for the spindle-bearing system.

Table 5 shows that the front bearing characteristics are subject to more difference between model 1 and model 2. However, unlike the front bearings, the rear bearing characteristics are less sensitive to changing the model. The reason why the rear two bearing characteristics are indifferent to switching model 1 to model 2 is that the reaction forces at the rear two bearings are almost identical to each other.

To emphasize the difference between two models, Fig. 11 shows natural frequencies of the spindle-bearing system with the rotational speed varied. Natural frequencies of model 2 are higher than those of model 1.

The reason is that tilting stiffness caused by two neighboring bearings is involved in model 2. This result claims the superiority of model 2 to model 1.

4. Concluding Remarks

This paper presented the dynamic analysis of indeterminate rotor systems with angular contact ball bearings. This paper proposed a finite element model and a new iterative algorithm for general, indeterminate rotor systems with angular contact ball bearings subject to axial and radial loads. An improved bearing model was adopted which is originated from the Harris's bearing dynamic model and is extended for including centrifugal forces in the balls and inner ring. To validate and illustrate the proposed method, two examples were provided. Through the examples, the proposed method was proved to be useful for the dynamic analysis of indeterminate rotor systems with angular contact ball bearings subjected to axial and radial loads. The results also showed that axial load increases bearing stiffness coefficients, and that ball centrifugal force (inner ring expansion) decreases (increases) bearing stiffness coefficients. This paper illustrated that static radial loads cause bearing anisotropy, which is believed to be important in the rotor dynamics point of view.

Acknowledgement

The first author wishes to acknowledge the financial support in 2000 by the research fund of Kumoh National University of Technology.

References

1. Jorgensen, B. R., "Dynamic Analysis of Spindle Bearing Systems," Ph.D Thesis, Purdue University, USA , 1997.
2. Reddy, W. R., and Sharan, A. M., "The finite element modeled design of lathe spindles: the static and dynamic analyses," Trans. ASME, Journal of Vibration, Acoustics, Stress and Reliability in Design, Vol.109, pp. 417-415, 1987.
3. Sadeghipuor, K. and Cowley, A., "The Effect of Viscous Damping and Mass-Distribution on the Dynamic Behavior of a Spindle-Bearing System," International Journal of Machine Tools and Manufacture, Vol. 26, No. 4, pp. 69-77, 1988.
4. Al-Shareef, K. J. H., and Brandon, J. A., "On the Effects of the Variations in the Design Parameters on the Dynamic Performance of Machine Tools Spindle Bearing Systems," International Journal of Machine Tools and Manufacture, Vol. 30, No. 3, pp. 432-445, 1990.
5. Brandon, J. A., and Al-Shareef, K. J. H., "Optimization Strategies for Machine Tool Spindle Bearing Systems: a Critical Review," Trans. ASME, Journal of Engineering for Industry, Vol. 114, pp. 244-253, 1992.
6. Wang, W. R., and Chang, C. N., "Dynamic Analysis and Design of a Machine Tool Spindle Bearing System," Trans. ASME, Journal of Vibration and Acoustics, Vol. 116, pp. 280-285, 1994.
7. Wang, K. W., Shin, Y. C. and Chen, C. H., "On the Natural Frequencies of High-Speed Spindles with Angular Contact Bearings," Proceedings of Institutions of Mechanical Engineering, Journal of Mechanical Engineering Science, Vol. 205, pp. 147-154, 1992.
8. Chen, C. H., Wang, K. W. and Shin, Y. C., "An Integrated Approach Toward the Dynamic Analysis of High Speed Spindles, Part 1: System Model," Trans. ASME, Journal of Vibration and Acoustics, Vol. 116, pp. 506-513, 1994.
9. Jorgensen, B. R., and Shin, Y. C., "Robust Modeling of High Speed Spindle Dynamics," Trans. ASME, Journal of Manufacturing Science and Engineering, Vol. 120, No. 2, pp. 387-394, 1998.
10. Shamine, D. M., Hong, S. W., and Shin, Y. C., "Experimental Identification of Dynamic Parameters of Rolling Element Bearings in Machine Tools," Trans.ASME, Journal of Dynamic Systems, Measurement and Control, Vol. 122, No. 1, pp. 95-101, 2000.
11. Harris, T. A., Rolling Bearing Analysis, New York: John Wiley & Sons , 1990.
12. Hagiu, G. D., and Gafitanu, M. D., "Dynamic Characteristics of High Speed Angular Contact Ball Bearings," Wear, Vol. 211, pp. 22-29, 1997.
13. Lee, C. W., and Hong, S. W., "Asynchronous Harmonic Response Analysis of Rotor-Bearing Systems," International Journal of Analytical and

Experimental Modal Analysis, Vol. 5, No. 2, pp. 51-65, 1990.

14. Hashish, E., and Sankar, T. S., "Finite Element and Modal Analyses of Rotor Bearing Systems under Stochastic Loading Conditions," Trans. ASME, Journal of Vibration, Acoustics, Stress and Reliability in Design, Vol. 106, pp. 890-898, 1984.
15. http://www.netlib.org/minpack